Letter

Microbubble Encapsulation by Electrostatic Templating with Ionic Surfactants

Vance Bergeron, Ramon Planet, and Stéphane Santucci*
Université Lyon, ENS de Lyon, CNRS, Laboratoire de Physique, Lyon F-69342, France

(Received 28 October 2021; revised 15 April 2022; accepted 26 April 2022; published 6 July 2022)

We propose an original microbubble encapsulation process, using electrostatics as a driving force to guide either particles or polymerizable precursors to the bubble surface. Taking advantage of attractive interactions between surfactant-laden charged bubbles and oppositely charged self-assembling species, our method produces capsules with diverse protective shells that remain stable for years. Considering heterogeneous electrostatic double-layer interactions, we quantitatively predict critical particle surface potentials required for complete encapsulation. The particle-based shells can be disintegrated with a pH adjustment, allowing for a controlled release of encapsulated payloads, while the glassy continuous silicate capsules are chemically resistant to pH changes. Our process, which can be equally applied to liquid droplets, easily scales up for industrial developments.

DOI: 10.1103/PhysRevApplied.18.L011001

Microbubbles display unique properties allowing the design of functional fluids relevant for many industrial processes [1] for ultrasound imaging [2], drug delivery [3], wastewater treatment [4], cosmetic creams, and food products [5–7]. However, they are intrinsically unstable: the pressure inside a microbubble follows Laplace's law, which drives Ostwald ripening. Consequently, microbubbles are short lived, typically lasting for only a matter of minutes, which severely limits their use [8].

To extend their lifetime, microbubbles can be encapsulated, to prevent the release of their content, while also providing elastic properties to their interface. Lipid, protein layers, or cross-linking organic polymers are commonly used but they produce soft nondurable shells that deflate over time [9,10]. Supramolecular architectures can encase emulsion drops and colloids, which upon removal of the internal phase create microcapsules [11–13]. Ultrasonic cavitation could also produce hollow mesoporous silica vesicles [14]. However, all of these methods do not generate long-lasting pressurized gas bubbles.

Originally exploited in flotation processes [15], and later reported by Ramsden [16] and Pickering [17], colloids attached to bubbles and oil drops have been observed to stabilize foams and emulsions [18–20]; a practice used in food and flotation industries for decades [21]. A factor contributing to particle adhesion and the subsequent dispersion stability is the particles' hydrophobicity characterized by their three-phase contact angle [22]. When around 90°, energy balances establish that particle detachment from a gas-water interface is orders of magnitude higher than k_BT [23]. However, limited complex chemical modifications of the colloids' surfaces are needed to adjust their wettability, which can be easily altered during postprocessing. Furthermore, predispersing hydrophobic particles for use in aqueous solutions requires also multiple steps and a high level of energy. Consequently, a viable protocol for large-scale production and postprocessing has yet to be developed.

Of note, from a fundamental perspective, the hydrophobic particle interaction with the dispersed phase before attachment is still not clearly understood. The existence of a yet to be elucidated "hydrophobic force" to breach the thin-liquid-film [24] that separates the particle from the dispersed phase interface is still debated [25,26]. While, recent advances in the measurement of a so-called "hydrophobic force" between bubble and particle have been obtained [26], a theoretical derivation from meaningful molecular parameters is still lacking. This ambiguity remains a central problem to a clear understanding of dispersions stabilized by hydrophobic particles.

Therefore, we propose in this Letter an original encapsulation process, using electrostatics interactions to drive either particles or polymerizable precursors to the bubble surface, and create a self-assembled encapsulating shell. Our general and simple approach can be quantitatively described by Derjaguin, Landau, Vervey, and Overbeek (DLVO) theory [27], considering heterogeneous electrostatic double-layer interactions [28]. Thus, it clarifies and circumvents the inherent difficulties and ambiguities of the so-called "Pickering" stabilization, allowing us to go beyond, by creating, at low cost and at industrial levels, a wide variety of *"bubbloons and droploids*," thanks to diverse protective shells, that strikingly remain stable

*stephane.santucci@ens-lyon.fr

for years. Furthermore, the particle-based capsules can be opened up with a pH adjustment, while using silicate anions as encapsulating species, the subsequent glassy continuous silicate shells are chemically resistant, and the encapsulation is irreversible.

The basis of our encapsulation process resides in the use of ionic surfactants that adsorb to the gas-liquid interface of the microbubbles, providing a residual charge to the bubble surface, so that oppositely charged species will be attracted to it. We first show in the following that DLVO theory [27] can explain and predict quantitatively when particle adhesion to an ionic surfactant-saturated bubble surface and thus, encapsulation occurs: the total potential energy of interaction V_T between a bubble and a particle in solution is given by the sum of their van der Waals, $V_d = -A_{132}(R_1R_2/6h(R_1+R_2))$, and dissimilar electrical double-layer interaction [28], $V_e = \frac{\varepsilon_o\varepsilon(\psi_1^2+\psi_2^2)R_1R_2}{4(R_1+R_2)}\left[\frac{2\psi_1\psi_2}{\psi_1^2+\psi_2^2}\ln\left(\frac{1+e^{-\kappa h}}{1-e^{-\kappa h}}\right)+\ln(1-e^{-2\kappa h})\right]$, with R_1, R_2 the bubble and particle radius, $\varepsilon_o\varepsilon$ the medium dielectric constant, ψ_1 and ψ_2 the surface potential of the bubble and particle, h the bubble-particle distance, A_{132} the composite Hamaker constant, and $1/\kappa$ the Debye length. Since $R_1 \gg R_2$, the interaction potential $V_T = V_e + V_d$ can be simplified,

$$\frac{V_T}{R_2} \simeq \frac{\varepsilon_o\varepsilon(\psi_1^2+\psi_2^2)}{4} \times\left[\frac{2\psi_1\psi_2}{\psi_1^2+\psi_2^2}\ln\left(\frac{1+e^{-\kappa h}}{1-e^{-\kappa h}}\right)+\ln(1-e^{-2\kappa h})\right] - \frac{A_{132}}{6h}.$$

We consider a well-characterized "ideal" case: a 100-μm-diameter air bubble in a cationic surfactant solution, such as hexadecyl trimethyl ammonium chloride (HTAC), at the critical micellar concentration, CMC $\simeq 10^{-3}$M, leading to a Debye length of 10 nm [27], and a surface potential of $\psi_1 \simeq +100$ mV [29], interacting with monodisperse silica spheres of $R_2 = 125$ nm radii. A composite Hamaker constant $A_{132} = -1\times10^{-20}$ J gives the repulsive van der Waals forces for the silica-water-air thin-liquid-film between the particles and bubble [30]. On the other hand, the particle surface potential depends on the pH of the solution. Using a ZetaPALS instrument, we measure how the surface potential of such silica particles evolves with the solution pH, as shown in Fig. 1(b). Successful bubble encapsulation occurred when the pH of the solution is larger than 4, corresponding to a drop in the particle surface potential lower than -40 mV. A cryo-SEM image [Fig. 1(c)] provides a typical example of such an encapsulated microbubble. In these conditions, the bubble-particle double-layer forces are sufficiently attractive to overcome van der Waals repulsion, decreasing the corresponding energy barrier to a value comparable to k_BT, as shown in Fig. 1(a); the particles will then spontaneously adhere to the bubble surface and subsequently encapsulate the bubble. This prediction for a critical particle surface potential is in excellent quantitative agreement with our experimental observations of bubble encapsulation and electrokinetic potential measurements, without any adjustable parameters, which is, remarkably, often not the case when attempts are made to use DLVO theory [31]. Interestingly, it also corresponds to experimental results reported in particle flotation studies [32].

The potential energy V_T is directly proportional to the particles size R_2. Thus, the smaller the particles, the lower the energy barrier. We display in Fig. 1(d), a 2D map showing how this energy barrier (computed as the maximum value $V_{\max}$ of V_T) evolves with both R_2 and the surface potential ψ_2, for this ideal test case of monodisperse silica spheres, interacting with a cationic surfactant saturated air bubble. Such a map gives the typical range, in terms of size and ζ potential of the particles used (R_2, ψ_2), for a successful encapsulation, depending also on the energy level one can provide. The isoline $V_{\max} = k_BT$ shows when the energy barrier is equal to Boltzmann thermal energy fluctuations. Up until this value, the particles will spontaneously adhere to the bubble surface; interestingly, for particles smaller than 50 nm, this barrier is always smaller than k_BT, even for low absolute value of their surface potential ψ_2, which can explain the ubiquitous observation of bubbles and droplets' stabilization with colloids. The encapsulation can also be facilitated by a more vigorous mixing, which could be required to encapsulate microbubbles with larger particles (up to a few μm, for instance) and/or particles with a lower absolute surface potential value.

To demonstrate the robustness of our encapsulation method, we have performed experiments with a variety of particles of different shapes (spheres, rods, needles, platelets), bulk materials (silica, boehmite, nacre), and either cationic (HTAC), or anionic [lauroyl sarcosinate (LS)] surfactant solutions at the CMC. Typical examples are shown Figs. 1 and 2. The bottom panel of Fig. 2 provides global macroscopic measurements of the volume of encapsulated microbubble dispersions (typically around 25 ml), arbitrarily chosen after 10 days, V_{10}, normalized by their initial volume (measured right after their formulation), V_0, as a function of the pH of the solution used. The bubbles are encapsulated either by silica spheres of around 100 nm (left panel), silica rods of approximately 100 nm long and 10 nm large (middle panel), and nacre platelets of few microns (right panel). The corresponding pH evolution of their electrokinetic potential ψ_2 is also displayed. The top panel of this figure, giving the volume of the stable encapsulated microbubble dispersions V_{10}/V_0 as a function of the surface potential of the encapsulating particles multiplied by the polarity of the ionic surfactant

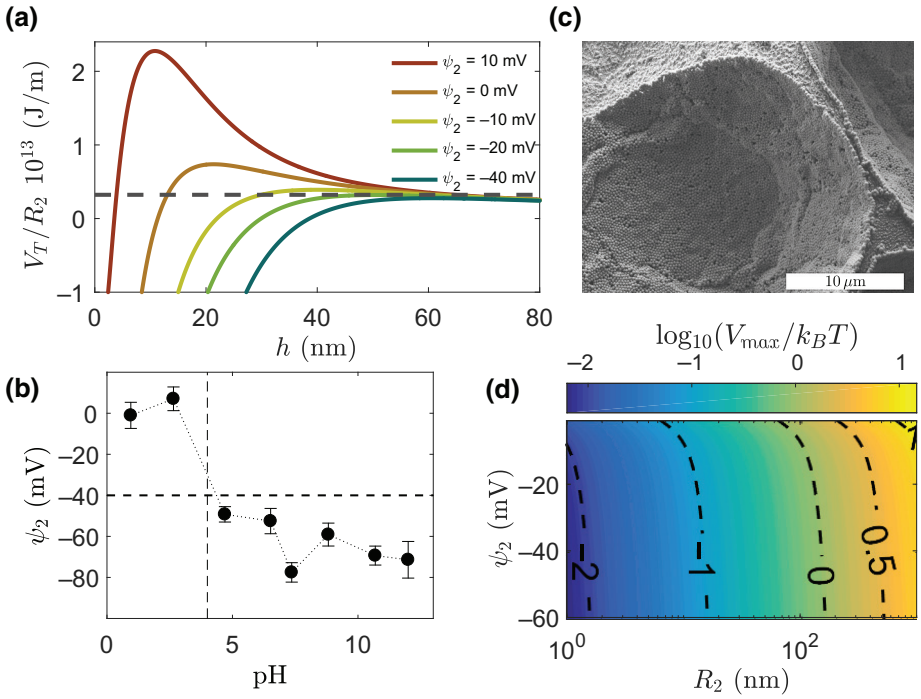

FIG. 1. (a) Bubble-particle interaction potential rescaled by the particle radius V_T/R_2 as a function of the distance h between the particle and the bubble surface, for the typical case of an air bubble dispersed in a solution of cationic surfactant, (bubble surface potential $\psi_1 \simeq +100$ mV), for various surface potentials ψ_2 of spherical silica particle of radius $R_2 = 125$ nm. The dashed line gives the value k_BT/R_2, at room temperature. (b) pH evolution of the surface potential of monodisperse silica particles of radius $R_2 = 125$ nm. A successful encapsulation is observed when the solution pH is larger than 4, corresponding to a surface potential ψ_2 lower than -40 mV. (c) A typical cryo-SEM image of such capsule. (d) Two-dimensional (2D) map of the energy barrier amplitude, renormalized by k_BT, in a logarithmic scale, $\log_{10}(V_{max}/k_BT)$ as a function of the radius of the silica spheres R_2, and their surface potential ψ_2. The dashed curves give various isolines.

head group, ψ_2^p, rationalizes our various measurements by providing a graphic representation of the surface potential criterion for encapsulating or liberating microbubbles with those various particles. We observe a distinct transition at a particle surface potential of around ± 40 mV where encapsulation occurs. It is remarkable that this experimentally determined value for a successful microbubble encapsulation is found for all of the various particles studied. However, the electrokinetic potential measurement (using electrophoretic mobility experiments) is indirect and based on a model that considers monodisperse spheres, while some of our samples are highly nonspherical (rods, platelets) and polydisperse. Nevertheless, the robustness of our findings clearly indicates that the double-layer forces play a predominant role in our electrostatic encapsulation process.

We demonstrate the general feature of our encapsulation process, showing that it can also be implemented with silicate precursor anions [33] instead of particles, and equally applied to liquid droplets. Typical microscopic images of such capsules are shown Fig. 3. As with particle encapsulation, we simply mix a sample of dispersed HTAC templated microbubbles with an equal volume of 0.1 M disodium metasilicate solution Na_2SiO_3, adjusted to pH 8.5 prior to use (approximately 30 s). Upon addition of acid, this stable alkaline solution (pH > 11) reacts with hydrogen ions to promote silicic acid polymerization, forming a glassy solid. The silicate anions attracted to the cationic surfactant head groups creates a solidified shell around the bubble interface. Unlike alkyloxysilanes, this rapid reaction at room temperature does not create alcoholic byproducts. Adjusting the silicate concentration, the shell thickness can be varied. Under our experimental conditions (60 vol% gas-bubble dispersions of around 50 μm diameter), at 0.1 M, the mean thickness can be estimated around 35 nm; while below, it is insufficient to completely cover the bubbles' surface. Further increases in disodium metasilicate molarity leads to simultaneous gelation of the excess metasilicate in solution, and even bubbles enclosed within a solid matrix, as shown in the Supplemental Material [36].

Once encapsulated our various microbubbles, which can be easily redispersed in solution, remain unchanged at room temperatures for months and years. Indeed, we demonstrate their extreme long-term stability by showing in Fig. 3(a) the temporal evolution of the volume of

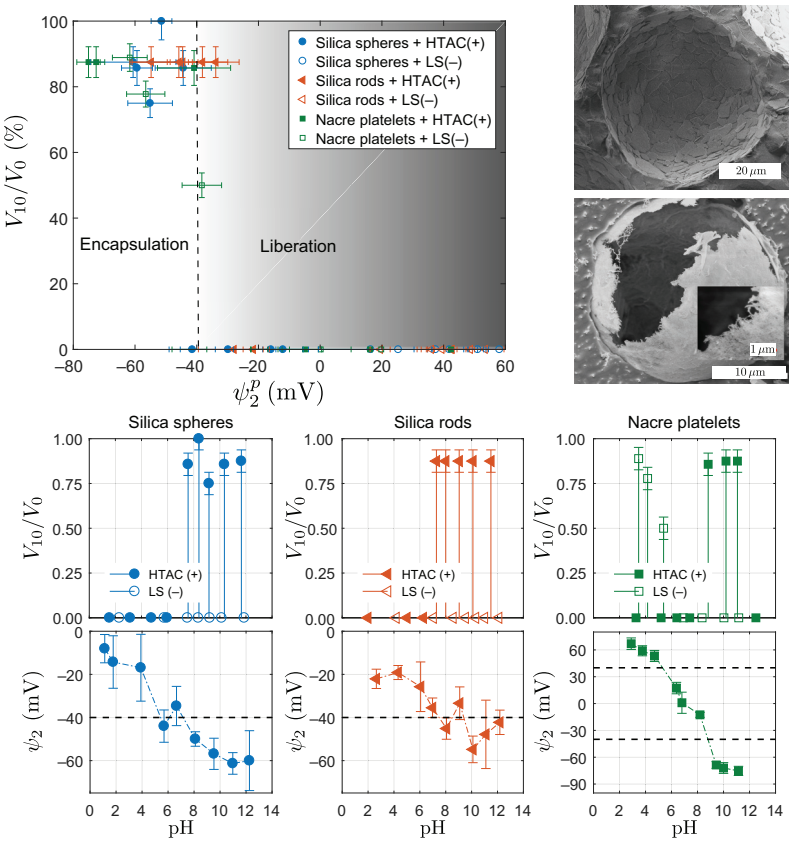

FIG. 2. Graphic representation of the particle surface potential criterion for encapsulating and liberating microbubbles, formulated with either cationic (HTAC) or anionic surfactants (LS), with different types of particles. The volume of stable microbubbles, arbitrarily chosen after 10 days, V_{10}, normalized by the initial volume, V_0, is plotted against the surface potential multiplied by the polarity of the ionic surfactant head group, ψ_2^p. A distinct transition at a potential of ± 40 mV is observed. Once encapsulated the microbubbles can be liberated by adjusting the solution pH to lower the surface potential of the particles. Bottom: evolution of the normalized volume of encapsulated microbubbles, V_{10}/V_0, and evolution of the electrokinetic potential of the encapsulating particles ψ_2, both, as a function of the pH of the solution used. Two cryo-SEM images present examples of encapsulated microbubbles with 100-nm-long boehmite needles, and micrometric nacre platelets.

different dispersions of microbubbles originally prepared with a cationic surfactant (HTAC) at CMC, encapsulated with different species (various particles or disodium metasilicate anions), renormalized by their initial volume V_0, around 25 ml. While the assembly of such microbubbles without any encapsulating protective shells shrinks very quickly (on minute time scales) and completely disappears in less than 2 h, by disproportionation and coalescence, the volume of our various samples of encapsulated microbubble dispersions remains equal to its initial value V_0 or shows only a slight decrease of a few percent after 2 months. Furthermore, a direct visual inspection of our samples up to 5 years confirmed that our various encapsulated samples remain strikingly unchanged, showing that our various formulated shells completely prevent and block the microbubbles; aging process. Interestingly, we also show in Fig. 3(b) that our electrostatic encapsulation process using particulate materials is reversible: with a pH adjustment bringing the pH values of their solution outside their respective encapsulating range (particle surface potential above -40 mV and below $+40$ mV), the particle-based shell capsules can be fragmented, and gas liberated, thus allowing the controlled release of encapsulated payloads. On the other hand, using polymerizable precursors (silicate anions) as encapsulating species, the subsequent glassy continuous silicate shells are chemically resistant, and the encapsulation is irreversible.

Finally, our encapsulation process can be easily upscaled for industrial developments [5,6]. It simply requires a stepwise procedure, where a free-flowing ionic surfactant-saturated bubble dispersion is produced first, and then simply mixed with oppositely charged species. An appropriate microbubble generation technique, allowing for a free-flowing bubble dispersion (gas volume fraction below 64%) to avoid interbubble adhesion with unrestricted access to the bubble surface of encapsulating species is indeed the first crucial step. As such, we have adopted a continuous stirred-tank reactor bubble generation process [34,35], shown in the Supplemental Material [36]. Then, our electrostatic encapsulation process simply requires that the number of ionic surfactants adsorbed to the bubble surface is greater than the ones in solution. Such a controlled partitioning ensures that any oppositely charged encapsulating species subsequently added to the gas-bubble dispersion will be attracted to the bubble surface, instead of being neutralized by free surfactants in solution. To determine this condition, we can estimate the adsorption density of surfactant over the particles' surface after microbubble formation by computing the ratio between the surfactant available in solution to the available particle surface area, $r = (N_S - N_{Sb})/N_p A_p$, with N_S the total number of surfactants, N_{Sb} the number of surfactants adsorbed to the bubble surface upon microbubble formation, A_p the surface area of the particle considered,

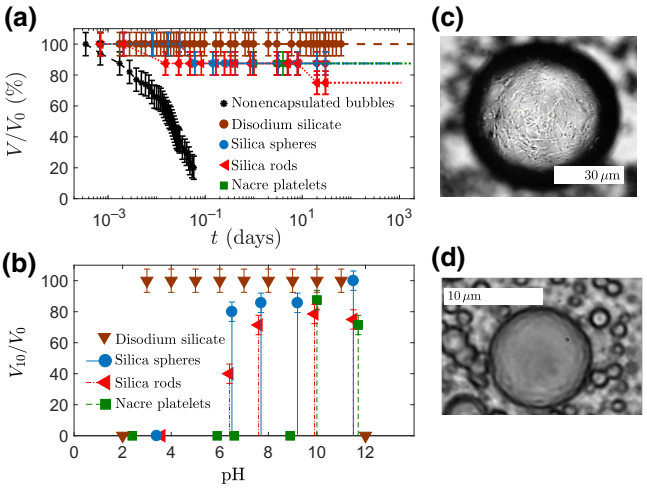

FIG. 3. (a) Temporal evolution of the volume V of microbubble dispersions prepared with HTAC cationic surfactants and encapsulated with either silica spheres, rods, nacre platelets, or polymerizable precursors (metasilicate anions), normalized by their initial volume V_0, systematically monitored from 1 min up to 3 months, and directly observed up to 5 years. (b) A pH-sweep over 10-day-old stable encapsulated microbubble dispersions (formulated with HTAC at the CMC) that shows the capsules can be fragmented and gas liberated, by adjusting the pH values of their solution outside their respective encapsulating range, bringing the particle surface potential above -40 mV and below $+40$ mV, for which, the global volume of the capsule dispersions drops. Optical microscope images of an air bubble (c) and a dodecane oil droplet (d), both encapsulated by a continuous silicate shell.

and N_p the number of particles. We can estimate this ratio r for spherical silica particles of various size in HTAC surfactant solutions at different concentrations used to generate 50 μm bubbles. A successful encapsulation occurs when $r \leq 0.75$ molecules/nm^2 (see Supplemental Material [36]). Such a result is in quantitative agreement with the measurement of Tyrode *et al.* [37], who could show that silica particles are not completely covered by the surfactants for such adsorption density values. Then, the oppositely charged particles can be attracted and attached to the bubble surface. If we exceed this coverage (increasing, for instance, the surfactant concentration), the particles will become partially hydrophobic, create hemimicelles [37], and aggregate to form flocs in solution, which subsequently prevents their attraction to the charged bubbles. Therefore, our encapsulation method is not due to an *in situ* modification of the particles' wettability: in contrast to the "Pickering" technique, we use hydrophilic particles.

To conclude, this Letter presents an original method for producing microcapsules. The "Pickering" stabilization of foams and emulsions with hydrophobic particles has been used for decades. However, the hydrophobic particle interaction with the surface of bubbles or droplets is still not clearly understood, and carrying out such a technique at an industrial scale is difficult. In stark contrast, our approach, which can be quantitatively described with DLVO theory, circumvents these difficulties. Therefore, we reveal an alternative way to guide self-assembly with electrostatics as the driving force, allowing the formulation of objects, stable for years, at low cost and at industrial levels, thanks to the creation of a diverse variety of protective shells. Indeed, our general and simple electrostatic encapsulation process can also be implemented with polymerizable precursor anions instead of particles, and applied to liquid droplets, thus paving the way to the formulation of more elaborate macroscopic structures. For instance, the use of metallic particles [38] can lead to the development of switchable photonic fluids, with plasmonic capsules [39] and liquid mirrors [40].

We thank S. Parola and F. Chaput for providing tailor-made nanoneedles, D. Chateau, E. Freyssingeas, C. Place, S. Parola, A. Asnacios, J.-T. Simonnet, A. Lafuma, F. Levy, for fruitful discussions and access to various equipments in their laboratories. V.B. wishes to dedicate this work to UC Berkeley Professors Clayton Radke and Douglas Fuerstenau, and the deceased Professors Felix Sebba and Pierre-Gilles de Gennes. This work is partially funded by L'Oreal, and ANR Tremplin ERC "PhoFo".

[1] J. Rodriguez-Rodríguez, A. Sevilla, C. Martínez-Bazan, and J. M. Gordillo, Generation of microbubbles with applications to industry and medicine, Annu. Rev. Fluid Mech. **47**, 405 (2015).
[2] M. Versluis, E. Stride, G. Lajoinie, B. Dollet, and T. Segers, Ultrasound contrast agent modeling: A review, Ultrasound Med. Biol. **46**, 2117 (2020).
[3] Y. Liu, H. Miyoshi, and M. Nakamura, Encapsulated ultrasound microbubbles: Therapeutic application in drug/gene delivery, J. Control. Release **114**, 89 (2006).
[4] A. Agarwal, W. J. Ng, and Y. Liu, Principle and applications of microbubble and nanobubble technology for water treatment, Chemosphere **84**, 1175 (2011).
[5] V. Bergeron, J. T. Simonnet, F. Levy, A. Lafuma, and S. Santucci, Bubble encapsulation via silicilic acid complexation, US patent 9, 452, 406 B2 (2016).
[6] V. Bergeron, J. T. Simonnet, F. Levy, A. Lafuma, and S. Santucci, Stable bubbles via particle absorption by electrostatic interaction, US patent 9, 433, 578 B2 (2016).
[7] F. L. Tchuenbou-Magaia, I. T. Norton, and P. W. Cox, in *Gums and Stabilisers for the Food Industry 15*, edited by P. A. Williams and G. O. Phillips (The Royal Society of Chemistry, Cambridge, UK, 2010), p. 113.
[8] C. E. P. Epstein and M. S. Plesset, On the stability of gas bubbles in liquid-gas solutions, J. Chem. Phys. **18**, 1505 (1950).
[9] M. M. Lozano and M. L. Longo, Microbubbles coated with disaturated lipids and DSPE-PEG2000: Phase behavior,

collapse transitions, and permeability, Langmuir **25**, 3705 (2009).
[10] E. Talu, M. M. Lozano, R. L. Powell, P. A. Dayton, and M. L. Longo, Long-term stability by lipid coating monodisperse microbubbles formed by a flow-focusing device, Langmuir **22**, 9487 (2006).
[11] F. Caruso, R. A. Caruso, and H. Mohwald, Nanoengineering of inorganic and hybrid hollow spheres by colloidal templating, Science **282**, 1111 (1998).
[12] O. D. Velev, K. Furusawa, and K. Nagayama, Assembly of latex particles by using emulsion droplets as templates. 1. Microstructured hollow spheres, Langmuir **12**, 2374 (1996).
[13] A. D. Dinsmore, M. F. Hsu, M. G. Nikolaides, M. Marquez, A. R. Bausch, and D. A. Weitz, Colloidosomes: Selectively permeable capsules composed of colloidal particles, Science **298**, 1006 (2002).
[14] R. K. Rana, Y. Mastai, and A. Gedanken, Acoustic cavitation leading to the morphosynthesis of mesoporous silica vesicles, Adv. Mater. **14**, 1414 (2002).
[15] C. J. Everson, Process of Concentrated Ores, US Patent 348, 157 A (1886).
[16] W. Ramsden, Separation of solids in the surface-layers of solutions and suspensions (observations on surface-membranes, bubbles, emulsions, and mechanical coagulation). Preliminary account, P. R. Soc. London **72**, 156 (1904).
[17] S. U. Pickering, CXCVI.-Emulsions, J. Chem. Soc. Trans. **91**, 2001 (1907).
[18] B. Binks and R. Murakami, Phase inversion of particle-stabilized materials from foams to dry water, Nat. Mater. **5**, 865 (2006).
[19] A. Cervantes Martinez, E. Rio, G. Delon, A. Saint-Jalmes, D. Langevin, and B. P. Binks, On the origin of the remarkable stability of aqueous foams stabilised by nanoparticles: Link with microscopic surface properties, Soft Matter **4**, 1531 (2008).
[20] N. Taccoen, F. Lequeux, D. Z. Gunes, and C. N. Baroud, Probing the Mechanical Strength of an Armored Bubble and Its Implication to Particle-Stabilized Foams, Phys. Rev. X **6**, 011010 (2016).
[21] E. Dickinson, Food emulsions and foams: Stabilization by particles, Curr. Opin. Colloid Interface Sci. **15**, 40 (2010).
[22] P. Finkle, H. D. Draper, and J. H. Hildebrand, The theory of emulsification, J. Am. Chem. Soc. **45**, 2780 (1923).
[23] A. F. Koretsky and P. M. I. Kruglyakov, Emulsifying effects of solid particles and the energetics of putting them at the water–oil interface, Izv. Sib. Otd. Akad. Nauk SSSR, Ser. Khim. Nauk **2**, 139 (1971).
[24] V. Bergeron, Disjoining pressures and film stability of alkyltrimethylammonium bromide foam films, Langmuir **13**, 3474 (1997).
[25] J. Ralston, D. Fornasiero, and N. Mishchuk, The hydrophobic force in flotation-a critique, Colloids Surf. A Physicochem. Eng. Asp. **192**, 39 (2001).
[26] Y. Xing, X. Gui, and Y. Cao, The hydrophobic force for bubble-particle attachment in flotation, Phys. Chem. Chem. Phys. **19**, 24421 (2017).
[27] J. N. Israelachvili, *Intermolecular and Surface Forces* (Academic press, London, 2011).
[28] R. Hogg, T. W. Healy, and D. W. Fuerstenau, Mutual coagulation of colloidal dispersions, T. Faraday Soc. **62**, 1638 (1966).
[29] S. Usui and H. Sasaki, Zeta potential measurements of bubbles in aqueous surfactant solutions, J. Colloid Interf. Sci. **65**, 36 (1978).
[30] R. F. Tabor, R. Manica, D. Y. C. Chan, F. Grieser, and R. R. Dagastine, Repulsive van der Waals Forces in Soft Matter: Why Bubbles Do Not Stick to Walls, Phys. Rev. Lett. **106**, 064501 (2011).
[31] M. Bostrom, D. R. M. Williams, and B. W. Ninham, Specific Ion Effects: Why DLVO Theory Fails for Biology and Colloid Systems, Phys. Rev. Lett. **87**, 168103 (2001).
[32] D. W. Fuerstenau, in *Froth flotation: A century of innovation*, edited by M. C. Fuerstenau, G. J. Jameson, and R. H. Yoon (Society for Mining, Metallurgy, and Exploration, Littleton CO, USA, 2007), p. 3.
[33] K. J. Edler, Soap and sand: Construction tools for nanotechnology, Phil. Trans. R. Soc. Lond. A **362**, 2635 (2004).
[34] F. Sebba, An improved generator for micron-sized bubbles, Chem. Ind. **3**, 91 (1985).
[35] D. L. Michelsen and F. Sebba, Microbubble Generator, US Patent 5, 314, 644 A (1994).
[36] See Supplemental Material at http://link.aps.org/supplemental/10.1103/PhysRevApplied.18.L011001 for additional details on the encapsulation process.
[37] E. Tyrode, M. W. Rutland, and C. D. Bain, Adsorption of CTAB on Hydrophilic Silica Studied by Linear and Nonlinear Optical Spectroscopy, J. Am. Chem. Soc. **130**, 17434 (2008).
[38] D. Chateau, A. Desert, F. Lerouge, G. Landaburu, S. Santucci, and S. Parola, Beyond the Concentration Limitation in the Synthesis of Nanobipyramids and Other Pentatwinned Gold Nanostructures, Appl. Mater. Interfaces **11**, 39068 (2019).
[39] C. Burel, A. AlSayed, L. Malassis, C. B. Murray, B. Donnio, and R. Dreyfus, Plasmonic-based mechanochromic microcapsules as strain sensors, Small **13**, 1701925 (2017).
[40] Y. Montelongo, D. Sikdar, Y. Ma, A. J. S. McIntosh, L. Velleman, A. R. Kucernak, J. B. Edel, and A. Kornyshev, Electrotunable nanoplasmonic liquid mirror, Nat. Mater. **16**, 1127 (2017).